



Applications of nuclear magnetic resonance (NMR) logging in tight sandstone reservoir pore structure characterization

Haitao Zhang¹ · Gaoren Li¹ · Haopeng Guo¹ · Wenjing Zhang¹ · Yanmei Wang¹ · Weibing Li¹ · Jinyu Zhou¹ · Changsheng Wang¹

Received: 15 January 2020 / Accepted: 18 June 2020 / Published online: 29 June 2020
© Saudi Society for Geosciences 2020

Abstract

Tight sandstone reservoir evaluation and characterization faced great challenge by using conventional well logging data due to the complicated pore structure. To improve tight sandstone reservoir identification, the pore structure should be first characterized. In this study, using the tight Chang 8 Formation of Pengyang Region, west Ordos Basin as an example, 20 core samples were drilled for laboratory nuclear magnetic resonance (NMR) and mercury injection capillary pressure (MICP) experiments. A model, which was used to construct capillary pressure (P_c) curves from NMR data, was proposed, and the corresponding models were established based on classified power function (CPF) method to classify formations into three types. Based on these relationships, the NMR T_2 distributions were transformed as pseudo P_c curves and pore throat radius distributions. After these relationships were extended into field applications, consecutive pseudo P_c curves were acquired, and the pore structure evaluation parameters and permeability were also predicted. Comparisons of predicted parameters with core-derived results illustrated the reliability of our proposed model and method.

Keywords Tight sandstone reservoirs · Pore structure · Nuclear magnetic resonance (NMR) data · Mercury injection capillary pressure (MICP) curve

Introduction

With the conventional reservoirs, which contained high porosity and permeability, further developed, the hydrocarbon potential was decreased. The unconventional reservoirs, such as shale oil/gas and tight oil/gas, had become the hotspot in oil and gas exploration due to the unlimited potential (Zou et al. 2012; Jia et al. 2016; Li et al. 2020a, b). The Chang 8 Formation of Ordos Basin, which was a typical tight sandstone reservoir (Fig. 1a–c), was recently ardently developed. To improve the development quality, accurately reservoir identification and evaluation were of great importance (Gao and Hu 2018; Liu et al. 2019; Zhu et al. 2019; Li et al. 2020a, b). However, plenty of field researches illustrated that tight

reservoir identification and evaluation of Chang 8 Formation are in-effective because it contained complicated pore structure. Many potential hydrocarbon-bearing formations were considered as dry layers or water saturated reservoirs (Xiao et al. 2011; Lis-Sledziona 2019). On the contrary, plenty of reservoirs, which were identified as water-bearing zones, were good hydrocarbon-bearing layers in production (Newberry et al. 1996; Ghafoori et al. 2009). To decrease these misdiagnoses, the pore structure of tight reservoirs should be first evaluated (Ge et al. 2014; Ge et al. 2015; Xiao et al. 2016a, b; Fournier et al. 2018; Puskarczyk et al. 2018; Krakowski 2019; Zhang et al. 2019; Zahid et al. 2019; Xiao et al. 2020).

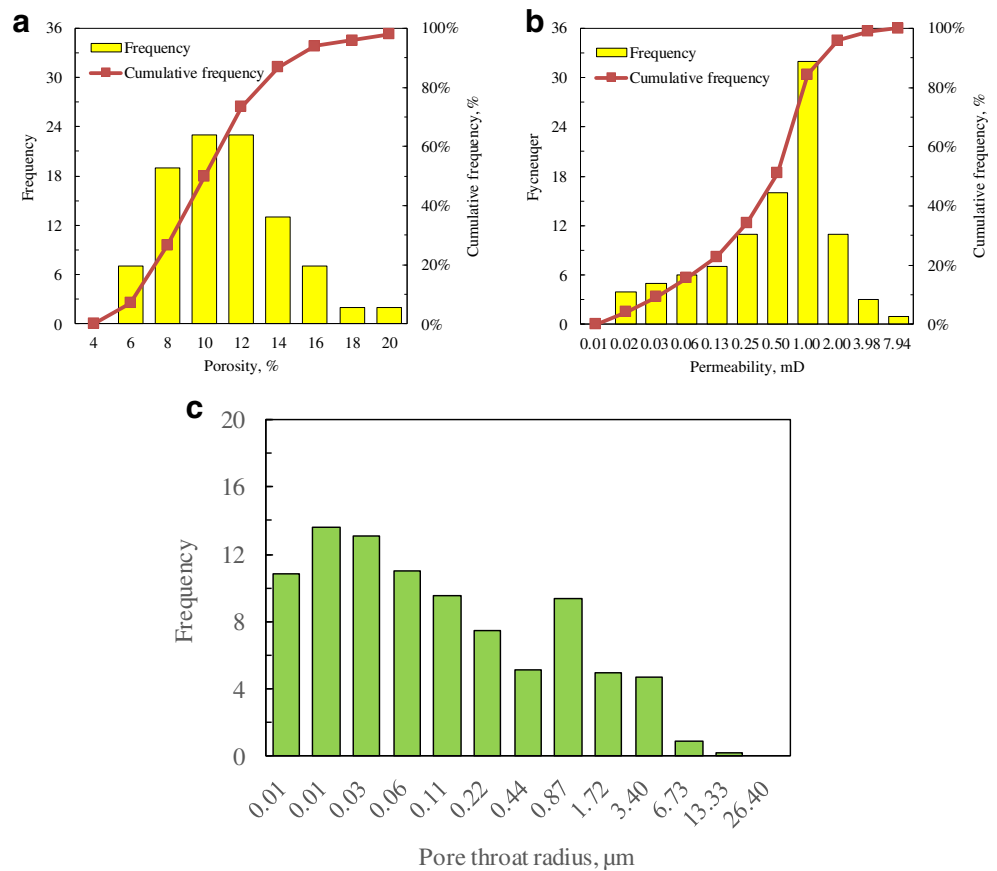
Plenty of methods were proposed to evaluate formation pore structure (Volokitin et al. 2001; Looyestijn 2001; Ouzzane et al. 2006; Olubunmi and Chike 2011). The most effective method and material of effectively characterizing formation pore structure was mercury injection capillary pressure (MICP) curve (Xiao et al. 2016a, b). From the MICP curves of core samples, many valuable information, such as the pore throat size distribution, the average pore throat radius, the maximal pore throat radius, and the threshold pressure, can be acquired. Based on these parameters, formations can be classified into several types,

Responsible Editor: Santanu Banerjee

✉ Haopeng Guo
cq15829469177@163.com

¹ Research Institute of Exploration & Development, Changqing Oilfield, PetroChina, Xi'an, Shaanxi, People's Republic of China

Fig. 1 The core-derived porosities (a), permeabilities (b), and pore throat radius statistical histograms (c) of the Chang 8 Formation in Pengyang Region, west Ordos Basin in China. These three figures illustrated that the porosities of the Chang 8 Formation ranged from 4.36 to 19.20%, the permeabilities ranged from 0.008 to 5.38 mD, and the pore throat radius mainly distributed from 0.01 to 0.87 μm . These illustrated that the Chang 8 Formation of our target region was a typical tight sandstone reservoir



and many hydrocarbon potential formations could be identified (Ge et al. 2015). Although the MICP curves were effective for pore structure evaluation, the quantity was limited because core samples were not consecutively drilled. Only limited core samples were drilled in the potential intervals. This led the pore structure cannot be consecutively characterized, and many uncored wells also cannot be evaluated.

The nuclear magnetic resonance (NMR) data was another valuable material to evaluate formation pore structure (Coates et al. 2000; Dunn et al. 2002). From the NMR transverse relaxation time T_2 distribution, the pore size and distribution can be qualitatively observed. However, the NMR data cannot be directly used to quantitatively characterize formation pore structure, because the pore throat size, but not the pore size, is the main factor that controls formation quality. To use the NMR data to characterize formation pore structure, many researchers pointed out that the NMR T_2 distribution should be processed and transformed as the pore throat radius distribution, and then pseudo-capillary pressure (P_c) curve (Volokitin et al. 2001; Xiao et al. 2012). To transform the NMR T_2 spectrum as pseudo P_c curve, several methods had been proposed. The most widely used methods contained linear scale function proposed by Volokitin et al. (2001) and nonlinear power function proposed by Xiao et al. (2016a, b). The linear scale function was easily used but the processed results were not reliable; the small

pore throat size cannot be reappeared. Xiao et al. (2012) also proposed another method based on the J function; several restricted conditions made it cannot be well used in field application. In this study, we tried all these methods in field applications, and the nonlinear power function proposed by Xiao et al. (2016a, b) was verified to be the most optimal.

Method and model

Relationship between T_2 time and P_c

Based on the principle of NMR logging, the transverse T_2 relaxation time is constructed by three parts: the bulk relaxation time T_{2B} , the surface relaxation time T_{2S} , and the diffusion relaxation time T_{2D} (Coates et al. 2000). The relationship among them can be expressed as follows:

$$\frac{1}{T_2} \approx \frac{1}{T_{2B}} + \frac{1}{T_{2S}} + \frac{1}{T_{2D}} \quad (1)$$

The relative importance of these three relaxation mechanisms depended on the property of saturated fluid in the pore spaces, pore size, surface relaxation strength, and rock surface wettability (Coates et al. 2000). Generally, for a water-

wettable rock, and fully saturated with brine, the values of T_{2B} and T_{2D} were ignored, and T_2 was dominated by T_{2S} . The value of T_{2S} was usually controlled by the pore size of rock. Hence, the T_2 relaxation time can be simplified as follows:

$$\frac{1}{T_2} \approx \frac{1}{T_{2S}} = \rho_2 \left(\frac{S}{V} \right)_{\text{por}} \tag{2}$$

where ρ_2 was the proportionality constant between $1/T_2$ and surface to volume ratio of the pore; S was the surface area of rock pore; V was the volume of rock pore; and S/V was called as the surface relaxivity. The subscript por stood for rock pore.

If rock pore shape was assumed as regular, Eq. 2 can be rewritten as follows:

$$\frac{1}{T_2} = \rho_2 \left(\frac{S}{V} \right)_{\text{por}} = F_S \frac{\rho_2}{r_{\text{por}}} \tag{3}$$

Based on the theory of capillary pressure, the relationship between capillary pressure and pore throat radius for air-mercury system can be expressed as follows (Purcell 1949):

$$P_c = \frac{0.735}{R_c} \tag{4}$$

where R_c was the pore throat size in micrometer.

If we assumed that the pore throat radius was related to the pore size, it can be expressed as follows:

$$r_{\text{por}} = m \times R_c \tag{5}$$

Combining Eqs. 3 and 4, a derived equation could be written as follows:

$$P_c = C \times \frac{1}{T_2} \tag{6}$$

or

$$R_c = C_{T_2 \rightarrow R_c} \cdot T_2 \tag{7}$$

where $C = \left(\frac{0.735n}{\rho_2 \times F_s} \right)$ was the transformation coefficient of P_c and T_2 , and $C_{T_2 \rightarrow R_c} = \frac{\rho_2 \times F_s}{n}$ was the transformation coefficient of R_c and T_2 .

Equations 6 and 7 illustrated that the T_2 relaxation time associated with P_c or R_c . The NMR T_2 relaxation time could be transformed as the P_c curve or pore throat radius distribution once the transformation coefficient C was first determined.

Establishment of model for constructing pseudo P_c curve from NMR data

To calibrate the value of C involved in Eq. 6 or 7 to construct pseudo P_c curve from NMR data, 20 core samples, which

were drilled from the Chang 8 Formation of Huangjiang Region, west Ordos Basin, were applied for NMR and MICP measurements. The experimental parameters were listed as follows: wait time (TW) 6.0 s, inter-cho spacing (TE) 0.2 ms, the number of echoes per echo train (NE) 4096, and the scanning number 128. The experimental results are listed in Table 1.

Swirr was the irreducible water saturation, R_{max} stood for the maximal pore throat radius, R_m was the average pore throat radius, R_{50} was the median pore throat radius, P_d was the threshold pressure, and P_{50} stood for the median pressure.

Based on the experimental results, the NMR T_2 distributions and MICP curves of the 20 core samples were acquired and displayed in Figs. 2 and 3, separately. These two figures illustrated that their pore structures were complicated. It was difficult to obtain a single function to establish the relationship between NMR and P_c curves. To establish a reliable relationship to relate P_c with T_2 , we tried to classify these core samples into three types based on the difference of rock physical properties. Three types of NMR T_2 spectra and the corresponding P_c curves are displayed in Figs. 4a–c and 5a–c, respectively.

Figures 4 and 5 illustrated that the shapes of T_2 distributions and MICP curves for every type of core samples were similar after they were classified into three types. In this condition, we could calculate an average T_2 distribution and MICP curve to represent all core samples within the same type.

In Figs. 6 and 7, we displayed the average T_2 spectra and MICP curves for the three types of core samples. From these two figures, we observed that the shapes and positions were correlated. For the first type of core samples, which represented the best pore structure, the NMR T_2 distribution lied to the right, and the large pore was dominated; the corresponding P_c curve lied to the bottom. As the pore structure deteriorated, the NMR T_2 distributions moved to the left, and the P_c curves raised to the top. This meant the core samples were reasonably classified. These three average T_2 spectra and P_c curves can be used to represent all 20 core samples.

To establish the transformational relation between NMR data and P_c curves, the NMR T_2 distributions were first processed and normalized to acquire the inverse cumulative curves, which contained similar shapes with the P_c curves. Figure 8 shows the three types of average inverse cumulative curves, those corresponded to the NMR distributions displayed in Fig. 6. Comparing Figs. 7 and 8, we observed that the shapes of the three types of average inverse cumulative curves were similar with those of the average P_c curves. However, their order of magnitudes were absolutely different. To transform the NMR T_2 distributions as pseudo P_c curves, relationships between Figs. 7 and 8 should be established, specifically.

Table 1 The NMR and MICP experimental results of 20 core samples

Core no.	The NMR experiments				The MICP experiments				
	Permeability (mD)	Porosity (%)	T_2 cutoff (ms)	Swirr (%)	R_{max} (μm)	R_m (μm)	R50 (μm)	Pd (MPa)	P50 (MPa)
T1	7.62	18.19	2.38	54.52	5.33	0.91	0.32	0.14	2.32
T2	31.25	16.82	11.10	51.52	13.36	2.94	0.60	0.06	1.24
T3	0.79	12.17	8.70	72.30	2.22	0.42	0.16	0.33	4.59
T4	2.80	15.46	4.20	65.77	2.22	0.45	0.18	0.33	4.11
T5	0.39	12.58	13.05	84.14	1.07	0.20	0.08	0.69	9.30
T6	0.02	5.90	1.15	82.81	0.54	0.10	0.02	1.37	45.94
T7	0.24	10.14	4.94	81.59	1.55	0.31	0.08	0.48	9.67
T8	4.55	12.59	5.35	55.28	3.85	0.69	0.20	0.19	3.75
T9	0.08	9.55	5.81	83.12	0.54	0.12	0.07	1.37	11.14
T10	0.01	4.75	3.29	81.83	0.36	0.08	0.04	2.05	16.70
T11	0.01	4.32	3.29	83.70	0.27	0.05	0.03	2.75	22.97
T12	0.37	14.68	12.03	84.64	1.58	0.27	0.06	0.47	12.67
T13	4.99	17.96	2.58	75.21	2.19	0.33	0.06	0.34	11.67
T14	0.001	3.82	6.83	92.74	0.11	0.03	0.02	6.87	49.00
T15	0.50	10.30	3.87	66.99	1.58	0.33	0.15	0.47	4.90
T16	0.97	15.36	6.29	76.30	0.71	0.19	0.09	1.03	7.99
T17	0.18	7.94	1.35	69.71	0.36	0.08	0.03	2.05	21.62
T18	0.71	10.57	2.03	67.63	2.27	0.41	0.13	0.32	5.49
T19	3.59	13.59	3.57	56.82	2.16	0.50	0.17	0.34	4.43
T20	0.59	10.42	6.29	88.15	0.73	0.14	0.07	1.01	10.35

To establish the relationship between P_c and T_2 time, the equisaturation principle was used to extract the T_2 time that corresponded to every P_c value under the same non-wettable saturation. Figure 9 displayed the principle of the equisaturation method.

By using the method displayed in Fig. 9, three types of average NMR inverse cumulative curves were processed,

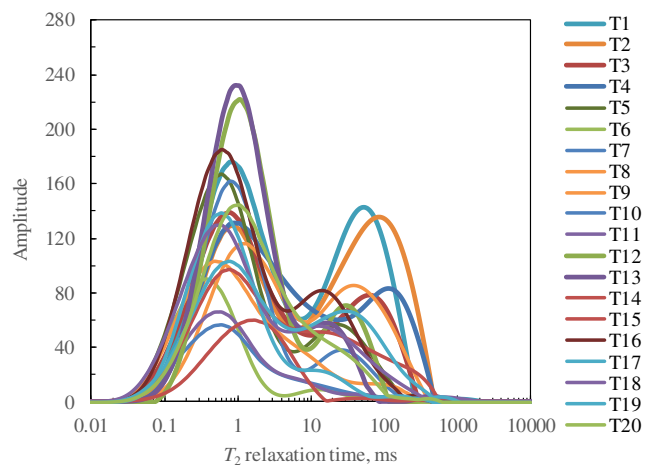


Fig. 2 The NMR T_2 distributions of 20 core samples. This figure illustrated that the small pore sizes were dominated in the Chang 8 Formation of Pengyang Region, west Ordos Basin, China

the those T_2 times corresponded to every P_c value were acquired and cross plotted with the P_c values, and the results illustrated that good power function relation existed among them. Meanwhile, based on the relationship between P_c and R_c displayed in Eq. 4, the relationship between P_c and T_2 was converted to R_c and T_2 , as is shown in Fig. 10.

By using the relationships displayed in Fig. 10, the NMR data can be processed and transformed as pseudo P_c curve.

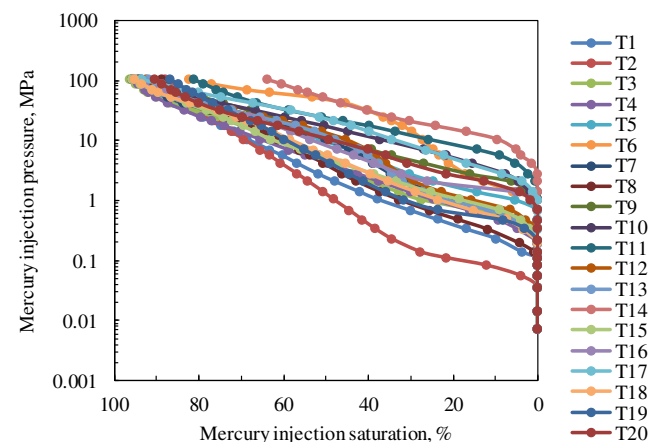


Fig. 3 The MICP curves of 20 core samples. The threshold pressures ranged from 0.08 to 7.0 MPa, and the maximal mercury injection saturations ranged from 61.50 to 94.30%

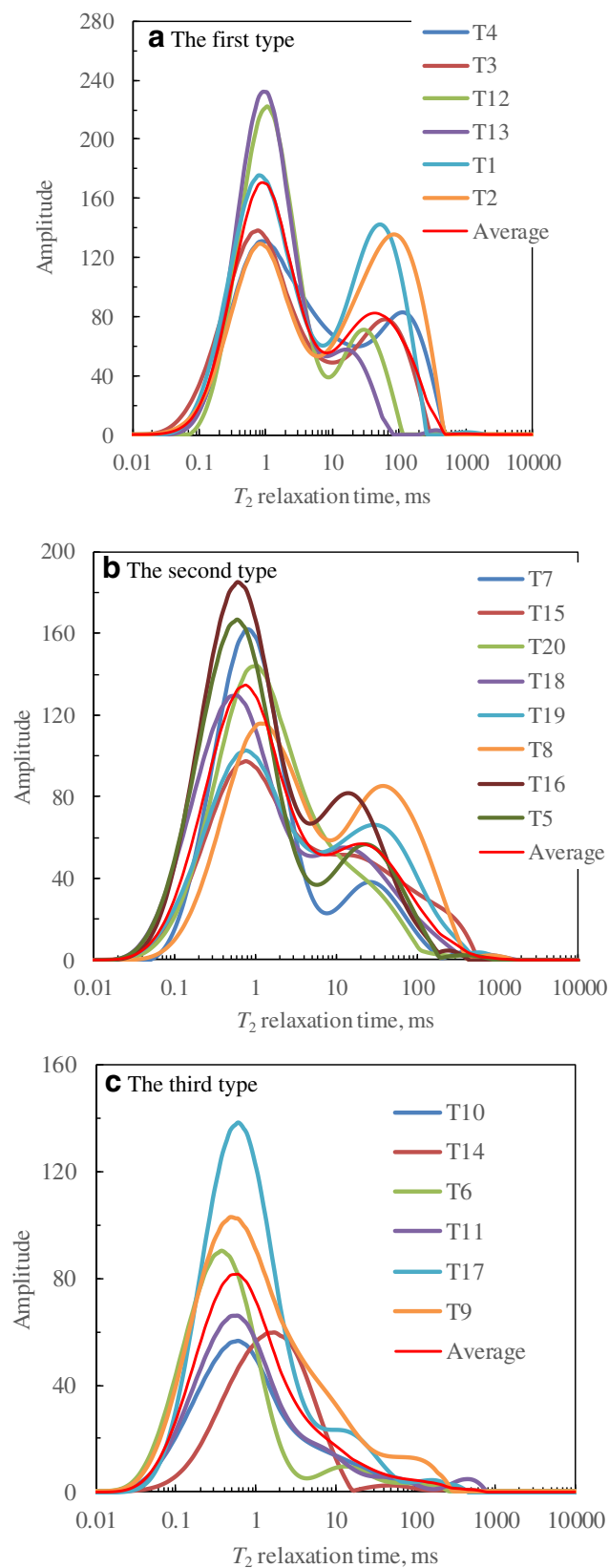


Fig. 4 Three types of NMR distributions. From the first type to the third type of rocks (a–c), the position of the main peaks moved to the left

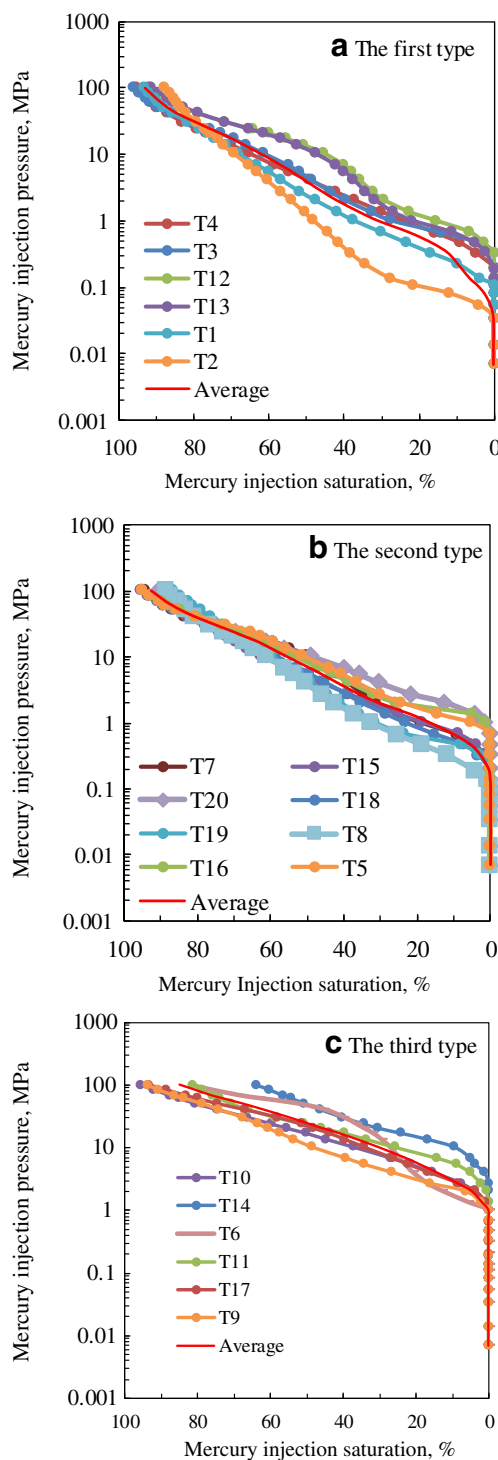


Fig. 5 Three types of MICP curves. From the first type to the third type (a–c), the represented rock pore structures became poorer and poorer

Once they were extended into field applications, field NMR logging can be processed, and consecutive pseudo P_c curves could be acquired in the intervals with which field NMR logging was acquired.

In Fig. 11, we displayed a field example of constructing pseudo P_c curves from field NMR logging in the Chang 8

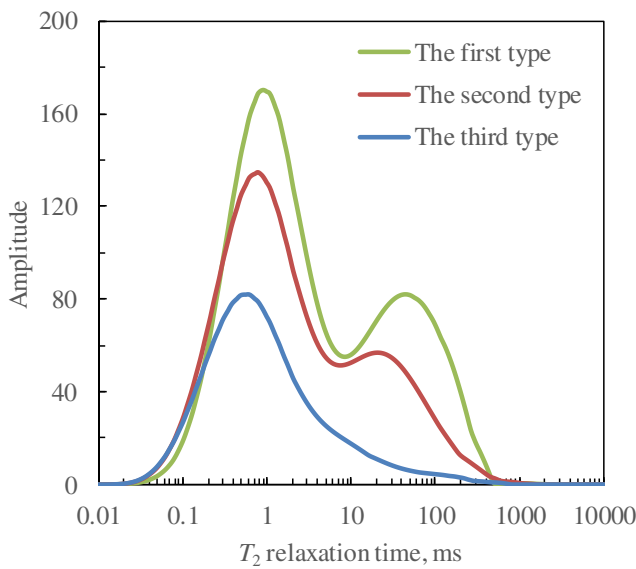


Fig. 6 Three types of average NMR distribution. From the first to the third type of rock, the average T_2 distribution became narrow, the position of the main peak moved to the left, and the shape of the T_2 spectrum became unimodality from bimodality

Formation, Huangjiang Region, west Ordos Basin. In the first three tracks in Fig. 11, we displayed the conventional well logging curves; they were used for identifying effective formation, estimating porosity, and indicating hydrocarbon-bearing formation. In the fourth track, we displayed the NMR T_2 distributions; the NMR data were acquired from Schlumberger’s CMR-Plus tool. In the fifth and sixth tracks, the constructed pseudo P_c curves and pore throat radius distributions were displayed. We displayed the comparison of permeabilities predicted from three different methods in the

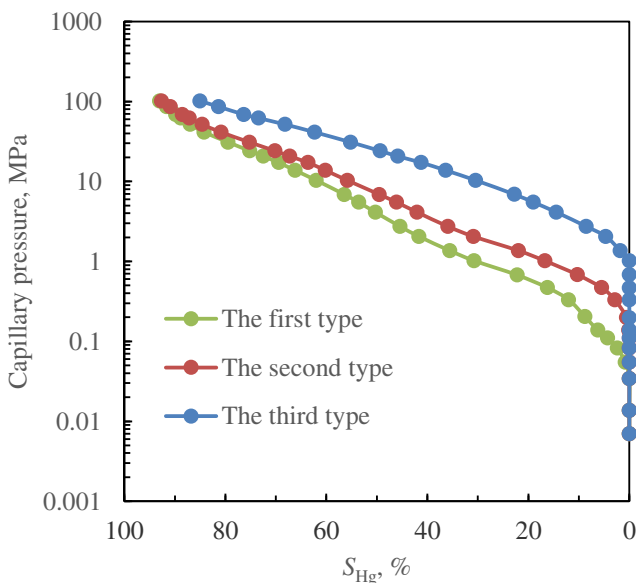


Fig. 7 Three types of average P_c curve. From the first to the third type of rock, the pore structure became poorer, and the morphologic trend was the same as the NMR T_2 spectra of the three types of rock

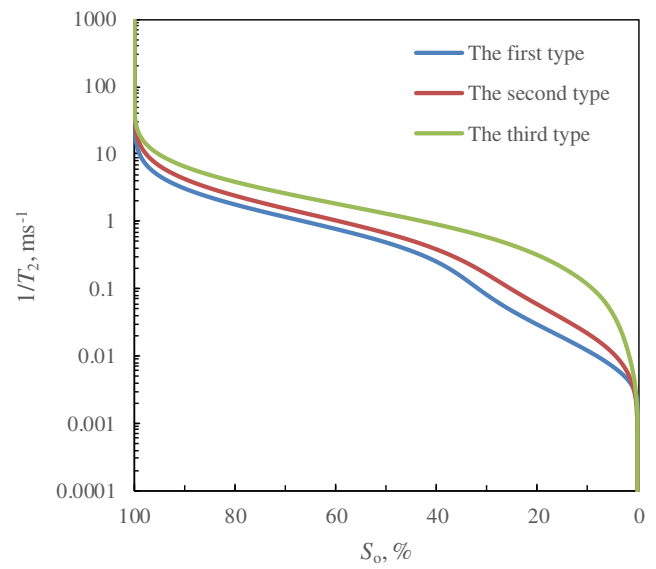


Fig. 8 Three types of average NMR inverse cumulative curves. The shapes of the average NMR inverse cumulative curves were similar with those of the average P_c curves displayed in Fig. 7, but the y-axis was absolutely different. The purpose of this study was to determine the optimal C to make Figs. 7 and 8 completely coincided

seventh track. PERMSWAN was the predicted permeability based on the Swanson parameter model established by Xiao et al. (2014). PERM was the estimated permeability curve from porosity based on the routine crossplot of core-derived porosity and permeability, and CPERM was the core-derived permeability. This comparison illustrated that the

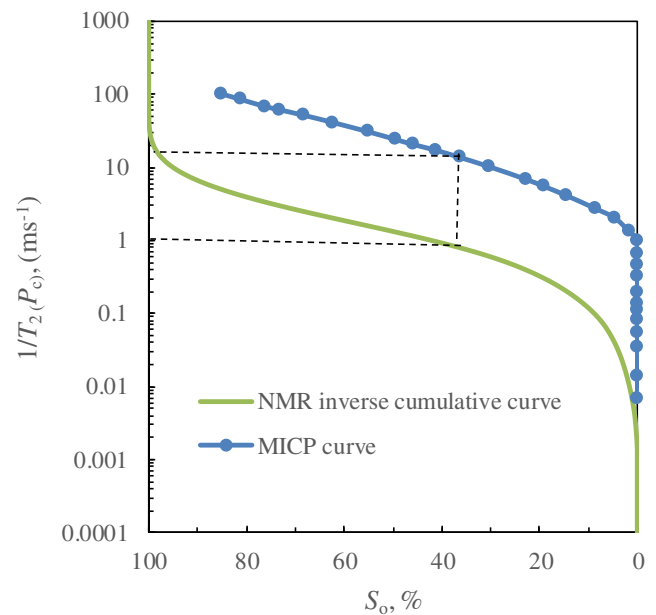


Fig. 9 Principle of acquiring the T_2 time that corresponded to every P_c . Based on the equisaturation method, a given non-wettable saturation was first determined. Next, a line, which passed the give non-wettable saturation and was perpendicular to the x-axis, was drawn. This line would both cross to the P_c and NMR inverse cumulative curve; the corresponded P_c and $1/T_2$ would be extracted

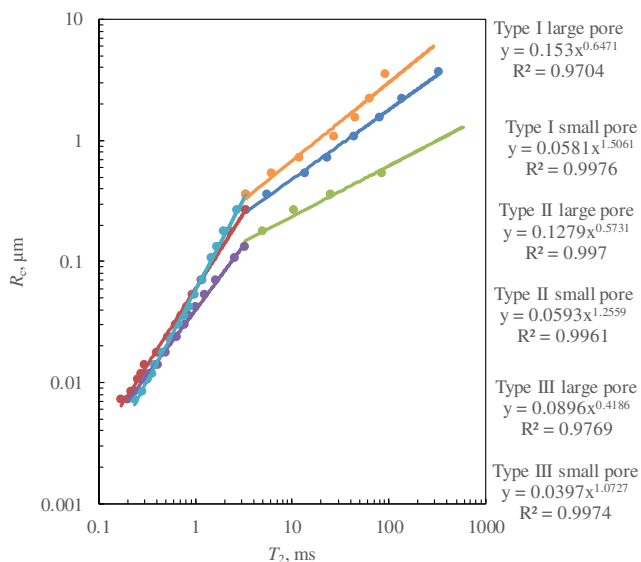


Fig. 10 Relationship between T_2 time and R_c for every type of formation

PERMSWAN was coincided with the core-derived permeability much well, while the permeability estimated by using the routine method was underestimated. The reason was that the PERMSWAN was predicted based on formation pore structure characterization (Xiao et al. 2017; Daigle et al. 2020). This meant that pore structure should be precisely characterized to predict permeability in tight sandstone reservoirs. In the last two tracks, we compared the predicted maximal pore throat radius (RMAX) and the median pore throat radius (R50) from pseudo P_c curves and derived from laboratory experimental results of core samples (CRMAX and CR50,

separately). The results illustrated that these two formation pore structure evaluation parameters were consistent. This meant that the constructed pseudo P_c curves were accurate and indirectly verified the reliability of the proposed method in this study.

Conclusions

Tight sandstone reservoirs cannot be directly estimated by using conventional methods due to the complicated pore structure. To improve tight sandstone reservoir evaluation, the pore structure should be first evaluated. The NMR logging was effective in evaluating formation pore structure once it was first transformed as the pseudo P_c curve.

The relationship between the T_2 time and the pore throat radius R_c was not a simple linear function, but a non-linear power function. To acquire reliable P_c curves from NMR logging, the classified power function method should be used. In the method, formation was first classified into three types, and for every type of rock, the power function was used to establish the relationship of T_2 time and pore throat radius.

In this study, 20 core samples recovered from the Chang 8 Formation in Huangjiang Region, west Ordos Basin, were used to calibrate the involved parameters in the proposed model, and a well was processed to verify the reliability. The result illustrated that the proposed method was available; it can be used to consecutively construct pseudo P_c curves from NMR logging in the intervals with which field NMR logging data was acquired.

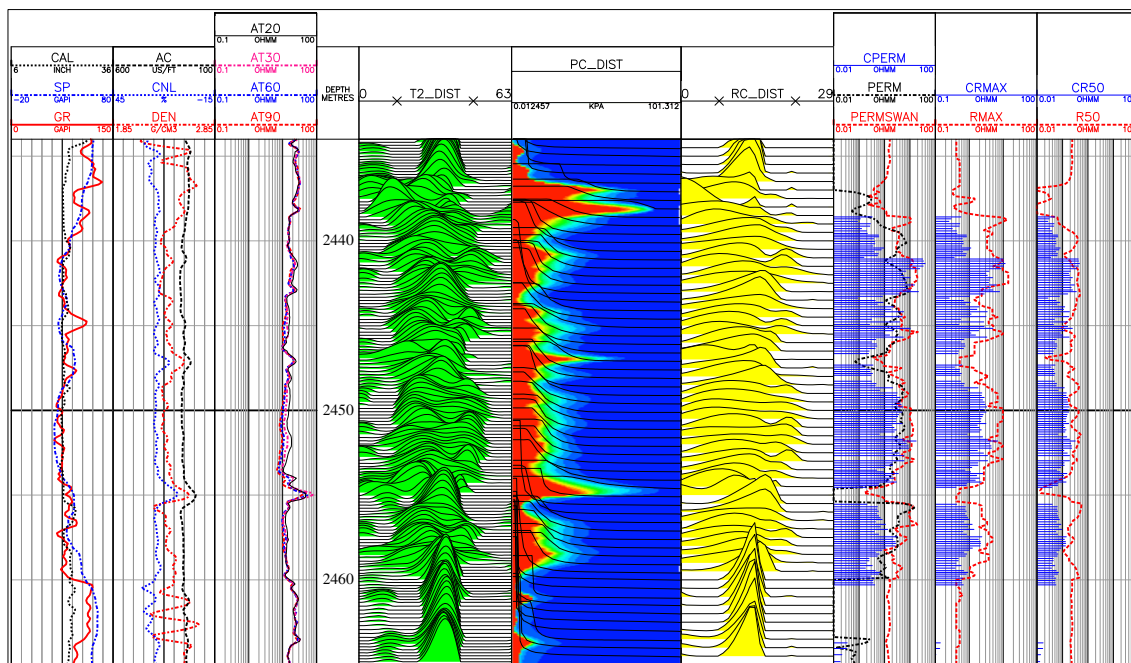


Fig. 11 A field example of constructing pseudo P_c curves and characterizing tight sandstone reservoir pore structure from NMR logging data by using the proposed method

Funding information This research was financially supported by the Major National Science and Technology Projects (2016ZX05050).

References

- Coates GR, Xiao LZ, Primmer MG (2000) NMR logging principles and applications: Houston, USA, Gulf Publishing Company, 256 p.
- Daigle H, Reece JS, Flemings PB (2020) A modified Swanson method to determine permeability from mercury intrusion data in marine muds. *Mar Pet Geol* 113:104115
- Dunn KJ, Bergman DJ, Latorraca GA (2002) Nuclear magnetic resonance: petrophysical and logging applications: New York, USA, Handbook of Geophysical Exploration, 176 p.
- Fournier F, Pellerin M, Villeneuve Q, Teillet T, Hong F, Poli E, Borgomano J, Léonide P, Hairabian A (2018) The equivalent pore aspect ratio as a tool for previous HitporeNext Hit type prediction in carbonate reservoirs. *AAPG Bull* 102(7):1343–1377
- Gao ZY, Hu QH (2018) Pore structure and spontaneous imbibition characteristics of marine and continental shales in China. *AAPG Bull* 102(10):1041–1061
- Ge XM, Fan YR, Cao YC, Xu YJ, Liu X, Chen YG (2014) Reservoir pore structure classification technology of carbonate rock based on NMR T2 spectrum decomposition. *Appl Magn Reson* 45(2):155–167
- Ge XM, Fan YR, Li JT, Zahid MA (2015) Pore structure characterization and classification using multifractal theory-An application in Santanghu basin of western China. *J Pet Sci Eng* 127:297–304
- Ghafoori MR, Roostaean M, Sajjadian VA (2009) Secondary porosity: a key parameter controlling the hydrocarbon production in heterogeneous carbonate reservoirs (case study). *Petrophysics* 50(1):67–78
- Jia CZ, Zheng M, Zhang YF (2016) Some key issues on the unconventional petroleum systems. *Pet Res* 1(2):113–122
- Krakowskal P (2019) Detailed parametrization of the pore space in tight clastic rocks from Poland based on laboratory measurement results. *Acta Geophys* 67(6):1765–1776
- Li CZ, Wang HH, Wang LG, Kang YM, Hu KL, Zhu YS (2020a) Characteristics of tight oil sandstone reservoirs: a case study from the Upper Triassic Chang 7 Member in Zhenyuan area, Ordos Basin, China. *Arab J Geosci* 13:78
- Li YL, Zhang YF, Fu H, Yan Q (2020b) Detailed characterization of micronano pore structure of tight sandstone reservoir space in three-dimensional space: a case study of the Gao 3 and Gao 4 members of Gaotaizi reservoir in the Qijia area of the Songliao basin. *Arab J Geosci* 13:119
- Lis-Sledziona A (2019) Petrophysical rock typing and permeability prediction in tight sandstone reservoir. *Acta Geophys* 67(6):1895–1911
- Liu GF, Bai YX, Gu DH, Lu Y, Yang DY (2019) Determination of static and dynamic characteristics of microscopic pore-throat structure in a tight oil-bearing sandstone formation. *AAPG Bull* 102(9):1867–1892
- Looyestijn WJ (2001) Distinguishing fluid properties and producibility from NMR logs. Proceedings of the 6th Nordic Symposium on Petrophysics, Trondheim, Norway, May 15–16, 2001, 9 p
- Newberry BM, Grace LM, Stief D (1996) Analysis of carbonate dual porosity systems from borehole electrical images: Permian Basin Oil and Gas Recovery Conference, Midland, Texas, USA, March 27–29, 1996, SPE-35158-MS, 7 p., doi: <https://doi.org/10.2118/35158-MS>.
- Olubunmi A, Chike N (2011) Capillary pressure curves from nuclear magnetic resonance log data in a deepwater turbidite Nigeria field—a comparison to saturation models from scale drainage capillary pressure curves. Nigeria Annual International Conference and Exhibition, Abuja, Nigeria, July 30–August 3, 2011, SPE-150749
- Ouzzane J, Okuyiga M, Gomaa N (2006) Application of NMR T2 relaxation to drainage capillary pressure in vuggy carbonate reservoirs: SPE Annual Technical Conference and Exhibition, San Antonio, Texas, USA, September 24–27, 2006, SPE-101897
- Purcell WR (1949) Capillary pressures—their measurement using mercury and the calculation of permeability therefrom. *Trans. AIME* 186: 39–48
- Puskarczyk E, Krakowska P, Jędrzychowski M, Habrat M, Madejski P (2018) A novel approach to the quantitative interpretation of petrophysical parameters using nano-CT: example of Paleozoic carbonates. *Acta Geophys* 66(6):1453–1461
- Volokitin Y, Looyestijn WJ, Slijkerman WFJ, Hofman JP (2001) A practical approach to obtain primary drainage capillary pressure curves from NMR core and log data. *Petrophysics* 42(4):334–343
- Xiao L, Mao ZQ, Shi YJ, Guo HP (2011) Analysis of “lower limit formation” in low permeability sands of Ordos Basin. SPE-139782
- Xiao L, Mao ZQ, Wang ZN, Jin Y (2012) Application of NMR logs in tight gas reservoirs for formation evaluation: a case study of Sichuan basin in China. *J Pet Sci Eng* 81:182–195
- Xiao L, Liu XP, Zou CC, Hu XX, Mao ZQ, Shi YJ, Guo HP, Li GR (2014) Comparative study of models for predicting permeability from nuclear magnetic resonance (NMR) logs in two Chinese tight sandstone reservoirs. *Acta Geophys* 62(1):116–141
- Xiao L, Mao ZQ, Zou CC, Jin Y, Zhu JC (2016a) A new methodology of constructing pseudo capillary pressure (Pc) curves from nuclear magnetic resonance (NMR) logs. *J Pet Sci Eng* 147:154–167
- Xiao L, Zou CC, Mao ZQ, Jin Y, Zhu JC (2016b) A new technique to synthesize capillary pressure (Pc) curves using NMR Logs in tight gas sandstone reservoirs. *J Pet Sci Eng* 145:493–501
- Xiao L, Liu D, Wang H, Li JR, Lu J, Zou CC (2017) The applicability analysis of models for permeability prediction using mercury injection capillary pressure (MICP) data. *J Pet Sci Eng* 156:589–593
- Xiao L, Li JR, Mao ZQ, Yu HY (2020) A method to evaluate pore structures of fractured tight sandstone reservoirs using borehole electrical image logging. *AAPG Bull* 104(1):205–226
- Zahid MA, Chunmei D, Golab AN, Lin CY, Zhang XG, Ge XM, Wu ST, Munawar MJ, Ma CF, Knuefing L (2019) Pore size distribution and reservoir characterization: evaluation for the Eocene beach-bar sequence, Dongying Depression, China. *Arab J Geosci* 12:660
- Zhang H, Zhu YS, Ma NY, Zhou CF, Dang YC, Shao F, Jiao J, Li L, Wang HL, Li M (2019) Combined technology of PCP and nano-CT quantitative characterization of dense oil reservoir pore throat characteristics. *Arab J Geosci* 12:534
- Zhu XJ, Cai JG, Liu Q, Li Z, Zhang XJ (2019) Thresholds of petroleum content and pore diameter for petroleum mobility in shale. *AAPG Bull* 103(3):605–617
- Zou CN, Zhang RK, Liu KY, Su L, Bai B, Zhang X, Yuan XJ, Wang JH (2012) Tight gas sandstone reservoirs in China: characteristics and recognition criteria. *J Pet Sci Eng* 88–89:82–91